Characterization of Transition Metal Dichalcogenide Nanostructures Synthesized by Liquid-Phase Controlled Fusion Technique

Alejandro Ramon Sanchez, Rafael Firas Montero *

Department of Physics, Faculty of Science, National University of Asuncion, Asuncion, PARAGRUAY
* Corresponding author email: dr.firas1990@yahoo.com

Abstract
In this letter, the synthesis of MoSSe nanosheets by liquid-phase controlled fusion technique is presented. The liquid-phase reaction of transition metal (Mo) with two chalcogenides (S and Se) was initiated in an inert environment and organic solvent. The synthesized material exhibited a polycrystalline structure with no traces for free elements or other phases than MoSSe and preferred parallel orientations, which confirmed the formation of nanosheets. Also, the elemental analysis showed that the synthesized material is sufficiently pure. The spectroscopic analysis confirmed the formation of all bonds required to form the MoSSe lattice. This attempt can be considered to synthesize nanosheets from hybrid systems based on transition metal and dichalcogenides.

Keywords: Nanostructures; Nanosheets; Dichalcogenides; Liquid-phase controlled fusion
Received: December 2025; **Revised:** January 2026; **Accepted:** February 2026; **Published:** April 2026

1. Introduction

In the recent years, the research interest in the 2D semiconductors, particularly the transition metal chalcogenides (TMDs), has increased due to their featured electronic and optical properties those are reasonably enhanced at the nanoscale [1-3]. These semiconductors have a general formula of MX_2, where M is a transition metal (such as molybdenum, tungsten, etc.) and X is a chalcogenide element (such as Sulphur, selenium, tellurium, etc.) [4-6]. These compounds show a radical conversion from the indirect energy bandgap in the bulk state to a direct energy bandgap when reduced to a single layer. As a result, they exhibit superior optical efficiency and ability to precise control of their characteristics [7-9].

With various nanostructures – such as nanosheets, nanoribbons, nanotubes, and quantum dots – fabricated from these materials, their applications are reasonable various to include advanced optoelectronics, sustainable catalysts, energy storage devices, and biosensors [10,11]. However, the largest challenge is the development of fabrication methods and techniques with sufficient capability to precise control of crystal dimensions (thickness, length and width), structural phase, and edge purity of these nanostructures, as these parameters are crucial in determining their final performance in the target application [12-14]. Accordingly, the liquid-phase synthesis techniques, particularly, the controlled fusion techniques, are interested as promising routes with flexibility, ability to develop, and precisely adjustable conditions [15-17].

The liquid-phase controlled fusion (LPCF) techniques exhibit new advantages over the conventional and limited-production techniques, such as chemical vapor deposition (CVD), which are carried at high temperatures and complex shape forming [18,19]. The LPCF technique mainly depends on fusion reactions between transition metal precursors and chalcogenides in a suitable organic solvent under precisely-controlled conditions (temperature and pressure) to allow dynamic control of growth process. Such process provides good control of formation rate of nanoparticles and their consecutive growth stages. This leads to produce structures with narrow size distributions and limited layer thickness. Furthermore, the reaction nature in solution allows using surface stability parameters (quenchers) and catalyst molecules to guide the growth preferentially in specific crystalline planes, and hence, the resulted nanostructures in desired shapes, such as 2D ultra-thin sheets or 1D ribbons [20-22]. This route allows forming hybrid homogeneous structures by adding precursors to the reaction medium. So, study of MX_2 nanostructures synthesized by the LPCF technique does not only concern to characterize the resulted materials but to understand the deep relationships between synthesis conditions (precursor chemistry, solvent state, temperature, reaction time, catalysis, etc.) and structural parameters (number of layers, sidewall

dimensions, geometry, crystalline defects, phase purity, etc.) [23-25].

In this work, the MoSSe nanosheets were synthesized by LPCF technique and their structural and morphological characteristics were introduced.

2. Experimental Part

The molybdenum dichloride ($MoOCl_2$) was used as a precursor for the transition metal, while Thiourea ($SC(NH_2)_2$) was used to produce the chalcogenide. All materials were prepared in an inert environment filled with argon because all precursors are very sensitive to oxidation and humidity. The organic solvent should be carefully selected to dissolve the different precursors with a boiling point suitable to the required reaction temperature (200-350°C). This solvent also works as a buffer for heat and mass transfer. The octadecane was used as the organic solvent, which shows high thermal stability.

The controlled fusion process was performed inside a glass reactor supplied with irreversible cooling condenser to prevent the solvent vaporization. This reactor was evacuated then filled with argon for three stages to ensure the complete exclusion of oxygen and water vapor from the reaction volume. The precursors were added to the solvent at accurate molar ratios of metal to chalcogenide (1:2) to produce chalcogenide-rich environment. The solution was heated and continuously stirred in a magnetic stirrer to ensure the homogeneity. Critical reaction mechanism was carefully followed to dissolve the precursors in the hot solvent in order to produce active buffer compounds. At 320°C, the growth process started as the metal precursors react with the chalcogenide to form the primitive small MX_2 molecules. The growth rate can be modified by the accurate control of heating curve (temperature increase rate and thermal stability durations) and modifying the solution viscosity via additional solvents. For instance, sodium chloride (NaCl) was added to modify the surface energy of specific crystalline planes to grow nanosheets with small thickness. As well, a small amount of distilled water was added to accelerate the reaction and encourage the formation of different structures.

After the completion of reaction (2 hours), the solution is rapidly cooled to room temperature in a water bath. Consequently, the nanoparticles were separated by adding an organic solvent (acetone) then centrifuged at 8000 rpm for 15 minutes. The resulted precipitate was washed several times with ethanol (polar) then hexane (non-polar) to remove the organic impurities, excess salts, and any unreacted stabilizing agents. Finally, the produced nanoparticles were dispersed in distilled water to form a homogeneous suspension for the next characterization measurements. This suspension can be stored in an inert environment at low temperature to maintain the stability of the synthesized nanomaterial and prevent its clustering and oxidation.

3. Results and Discussion

Figure (1) shows the XRD pattern of the synthesized MoSSe nanosheets. This pattern is dominated by the (002) crystal plane, which is the preferred growth orientation parallel to the direction of 2D layers. The high intensity of the (002) peak when compared to other peaks reveals that the synthesized nanomaterial is fundamentally composed of thin sheets with high parallel alignment. This agrees with the main goal of LPCF technique used to prepare 2D materials. The (006) peak support this assumption of reflection from serial crystalline planes within the same orientation of crystalline group. This confirms the consecutive layer structure of MoSSe.

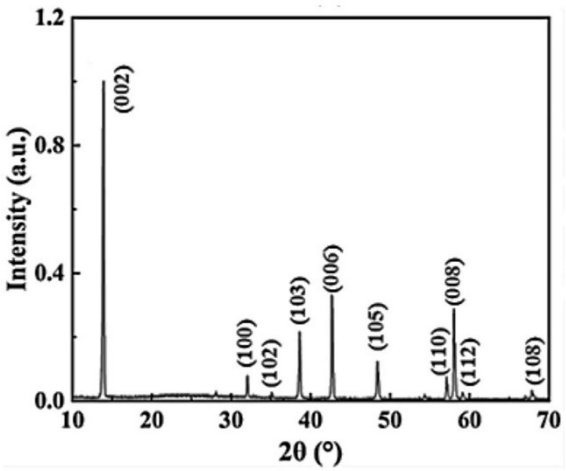

Fig. (1) XRD pattern of the MoSSE nanosheets synthesized by LPCF technique in this work

Appearance of other peaks such as (103), (110), and (112) – even though with lower intensities – refers to the polycrystalline structure of the material, and hence to the synthesis process, which was not able to achieve complete crystal orientation in all nanoparticles. This may be attributed to the reaction conditions or the locally inhomogeneous rates. This pattern reveals that no apparent crystal impurities were detected from pure molybdenum, selenium, or Sulphur [26]. In general, the XRD pattern confirms the success of the LPCF technique to synthesize hexagonal WSSe structure as high-quality nanosheets.

Figure (2) shows the EDS spectrum of the MoSSe nanosheets synthesized in this work. This spectrum shows apparent peaks of the Mo, Se, and S elements, which confirms the constitution of the synthesized material from these elements. The detection of two separate peaks of S and Se reveals the formation of ternary compound (MoSSe) instead of individual pure MoS_2 or $MoSe_2$ phases. However, the relative

intensities refer to a complex structure. The higher intensity of S peak when compared to that of Se may reveal that the two chalcogenides (S and Se) are not equivalent in the produced structure, or they are affected by the tuning efficiency of the X-ray as well as the atomic absorption of each element [27-29]. Therefore, an accurate quantum characterization with reference standards is crucially required.

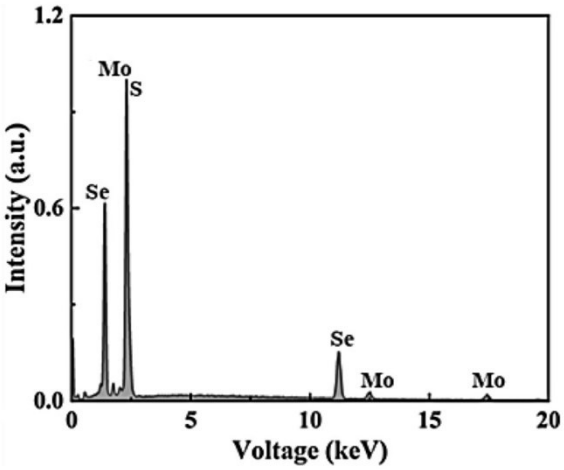

Fig. (2) EDS spectrum of the WSSE nanosheets synthesized by LPCF technique in this work

The Raman spectrum shown in Fig. (3) for the MoSSe nanosheets synthesized in this work reveals its hybrid structure and 2D layers. A complex pattern is shown and ascribed to the combined effects of MoS_2 and $MoSe_2$ vibrations due to the asymmetric formation of S-Se chalcogenide alloy. An intense and apparent peak is observed at 2500 cm^{-1}, which is not conventional for dichalcogenide lattices. This may refer to the existence of a secondary peak, a signal related to fluorescence, or a limited thickness of the formed layer. Also, vibration bands are observed in the low (125-175 cm^{-1}) and high (250-300 cm^{-1}) regions of the spectrum, as the hybrid configurations are recognized. Typically, two main peaks are expected to appear at ~383 cm^{-1} ascribed to MoS_2 and at ~289 cm^{-1} ascribed to $MoSe_2$, with a third peak in between the former peaks. The overall distribution of intensity within 150-450 cm^{-1} agrees with these expectations as the shifting and broadening when compared to the pure materials refers to the formation of Mo-S-Se bon. The absence of peaks ascribed to MoS_2 and $MoSe_2$ bond vibrations support the assumption of forming homogeneous alloy not a mechanical mixture from both phases. Moreover, the broadening in peaks refers to a possibility of a disturbance in the crystal lattice or a difference in the number of layers, which is common in nanomaterials prepared from liquid phase [30].

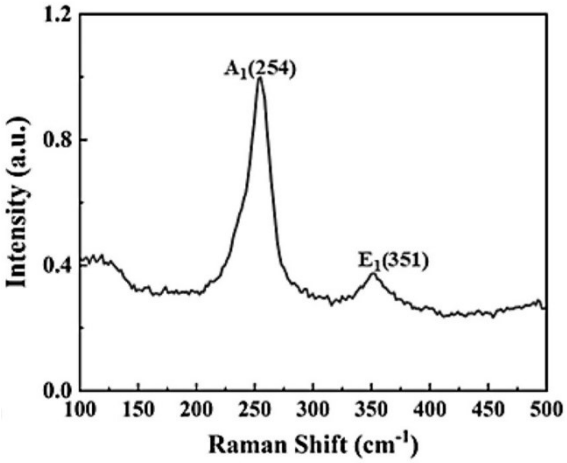

Fig. (3) Raman spectrum of the WSSE nanosheets synthesized by LPCF technique in this work

4. Conclusion

In conclusions, The synthesized MoSSe material exhibited a polycrystalline structure with no traces for free elements or other phases than MoSSe and preferred parallel orientations, which confirmed the formation of nanosheets. Also, the synthesized material is sufficiently pure. All bonds required to form the MoSSe lattice were formed. This attempt can be considered to synthesize nanosheets from hybrid systems based on transition metal and dichalcogenides.

References

[1] J. Chen and W. Xu, "2D-materials-based optoelectronic synapses for neuromorphic applications", *eScience*, 3(6) (2023) 100178.

[2] S.S. Jolly et al., "Quantum optics in photocatalytic hydrogen production: Light-matter interaction at the quantum scale", *Next Nanotech.*, 9 (2026) 100355.

[3] H. Yin et al., "The data-intensive scientific revolution occurring where two-dimensional materials meet machine learning", *Cell Rep. Phys. Sci.*, 2(7) (2021) 100482.

[4] A. Raza et al., "Strategies for robust electrocatalytic activity of 2D materials: ORR, OER, HER, and CO2RR", *Mater. Today Adv.*, 22 (2024) 100488.

[5] E. Llobet, "Transition metal dichalcogenide based toxic gas sensing", *Curr. Opin. Environ. Sci. Health*, 37 (2024) 100533.

[6] S. Lakshmy et al., "Recent developments in synthesis, properties, and applications of 2D Janus MoSSe and $MoSe_xS_{(1-x)}$ alloys", *Adv. Powder Mater.*, 3(4) (2024) 100204.

[7] E. Ghazanfar et al., "Ternary composites based next-generation supercapacitors electrode material: Emerging trends", *Electrochem. Commun.*, 174 (2025) 107893.

[8] G.A. Naikoo et al., "2D materials, synthesis, characterization and toxicity: A critical review", *Chemico-Biol. Interact.*, 365 (2022) 110081.
[9] K.R. Wijaya et al., "2D transition metal dichalcogenides for photovoltaics, hydrogen production, and CO_2 photoreduction", *RSC Sustain.*, 3(11) (2025) 4887-4910.
[10] A.K. Yadav et al., "Polyaniline (PANI) nanocomposites with Se, Te and their metal chalcogenides: a review", *RSC Appl. Polym.*, 2(5) (2024) 775-794.
[11] S. Palchoudhury et al., "Transition metal chalcogenides for next-generation energy storage", *Nanoscale Adv.*, 5(10) (2023) 2724-2742.
[12] H. Li et al., "Atomic-scale characterization of structural heterogeny in 2D TMD layers", *Mater. Adv.*, 3(3) (2022) 1401-1414.
[13] A. Bandyopadhyay, N.B. Joseph, and A. Narayan, "Non-linear Hall effects: Mechanisms and materials", *Mater. Today Electron.*, 8 (2024) 100101.
[14] J. Wang et al., "Controlled growth of atomically thin transition metal dichalcogenides via chemical vapor deposition method", *Mater. Today Adv.*, 8 (2020) 100098.
[15] W.-J. Yin et al., "Recent advances in low-dimensional Janus materials: theoretical and simulation perspectives", *Mater. Adv.*, 2(23) (2021) 7543-7558.
[16] N.B. Bakranov et al., "SiC-based heterostructures and tandem PEC cells for efficient hydrogen production", *Result Eng.*, 27 (2025) 106862.
[17] J.H. Zhuang et al., "Recent progress in two-dimensional materials: From emerging structures and synthesis approaches to electronic and sensing applications", *Chem. Eng. J.*, 520 (2025) 166133.
[18] M. Gu et al., "Molecular modulation strategies for two-dimensional transition metal dichalcogenide-based high-performance electrodes for metal-ion batteries", *Chem. Sci.*, 15(7) (2024) 2323-2350.
[19] C. Verma, A. AlFantazi and C.M. Hussain, "Chemical strategies and structural designs of Janus materials for corrosion resistance: Advances & perspectives", *Adv. Colloid Interface Sci.*, 348 (2026) 103729.
[20] G. Song, S. Cong and Z. Zhao, "Defect engineering in semiconductor-based SERS", *Chem. Sci.*, 13(5) (2022) 1210-1224.
[21] J. Liang et al., "Atomic Arrangement Engineering of Metallic Nanocrystals for Energy-Conversion Electrocatalysis", *Joule*, 3(4) (2019) 956-991.
[22] A.K. Singh et al., "Review of strategies toward the development of alloy two-dimensional (2D) transition metal dichalcogenides", *iScience*, 24(12) (2021) 103532.
[23] S. Rana, V. Singh and B. Singh, "Recent trends in 2D materials and their polymer composites for effectively harnessing mechanical energy", *iScience*, 25(2) (2022) 103748.
[24] S. Fu et al., "Tracking and controlling ultrafast charge and energy flow in graphene-semiconductor heterostructures", *The Innovation*, 6(3) (2025) 100764.
[25] L. Bignardi et al., "Exploring 2D materials at surfaces through synchrotron-based core-level photoelectron spectroscopy", *Surf. Sci. Rep.*, 78(1) (2023) 100586.
[26] W. Li et al., "Interlayer interactions in transition metal dichalcogenides heterostructures", *Rev. Phys.*, 9 (2022) 100077.
[27] Y. Sim, Y. Chae and S.-Y. Kwon, "Recent advances in metallic transition metal dichalcogenides as electrocatalysts for hydrogen evolution reaction", *iScience*, 25(10) (2022) 105098.
[28] W. Wang et al., "Defect engineering in molybdenum-based electrode materials for energy storage", *eScience*, 2(3) (2022) 278-294.
[29] B. Kirubasankar et al., "Atomic and structural modifications of two-dimensional transition metal dichalcogenides for various advanced applications", *Chem. Sci.*, 13(26) (2022) 7707-7738.
[30] S. Mehta et al., "Recent advances in ternary transition metal dichalcogenides for electrocatalytic hydrogen evolution reaction", *Int. J. Hydrogen Ener.*, 82 (2024) 1061-1080.

